Temperature Rise of Silicon Due to Absorption of Permeable Pulse Laser

Etsuji Ohmura
Osaka University
Japan

1. Introduction

Blade dicing is used conventionally for dicing of a semiconductor wafer. Stealth dicing (SD) was developed as an innovative dicing method by Hamamatsu Photonics K.K. (Fukuyo et al., 2005; Fukumitsu et al., 2006; Kumagai et al., 2007). The SD method includes two processes. One is a "laser process" to form a belt-shaped modified-layer (SD layer) into the interior of a silicon wafer for separating it into chips. The other is a "separation process" to divide the wafer into small chips. A schematic illustration of the laser process is shown in Fig. 1.

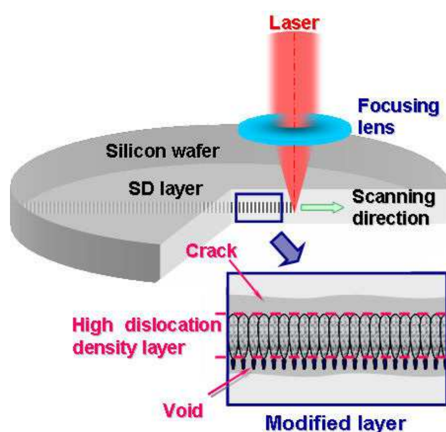

Fig. 1. Schematic illustration of "laser process" in Stealth Dicing (SD)

When a permeable nanosecond laser is focused into the interior of a silicon wafer and scanned in the horizontal direction, a high dislocation density layer and internal cracks are formed in the wafer. Fig. 2 shows the pictures of a wafer after the laser process and small chips divided through the separation process. The internal cracks progress to the surfaces by applying tensile stress due to tape expansion without cutting loss. An example of the photographs of divided face of the SD processed silicon wafer is shown in Fig. 3.

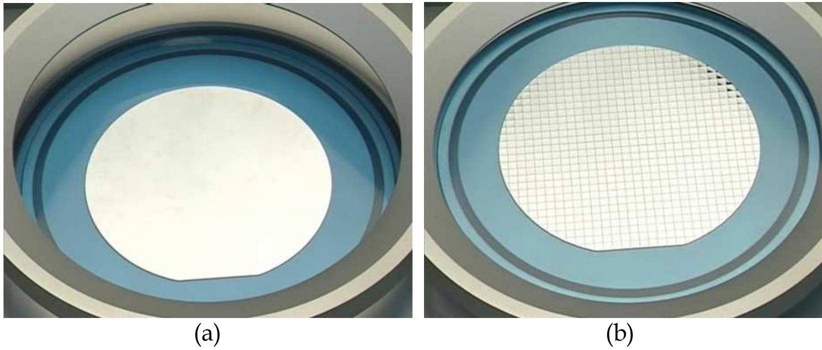

Fig. 2. A wafer after the laser process (a) and small chips divided through the separation process (b) (Photo: Hamamatsu Photonics K.K.)

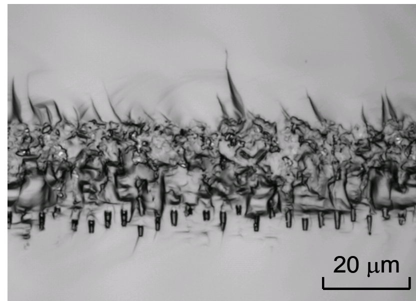

Fig. 3. Internal modified layer observed after division by tape expansion

As the SD is a noncontact processing method, high speed processing is possible. Fig. 4 shows a comparison of edge quality between blade dicing and SD. In the SD, there is no chipping and no cutting loss, so there is no pollution caused by the debris. The advantage of using the SD method is clear. Fig. 5 shows an example of SD application to actual MEMS device. This device has a membrane structure whose thickness is 2 μm, but it is not damaged. A complete dry process of dicing technology has been realized and problems due to wet processing have been solved.

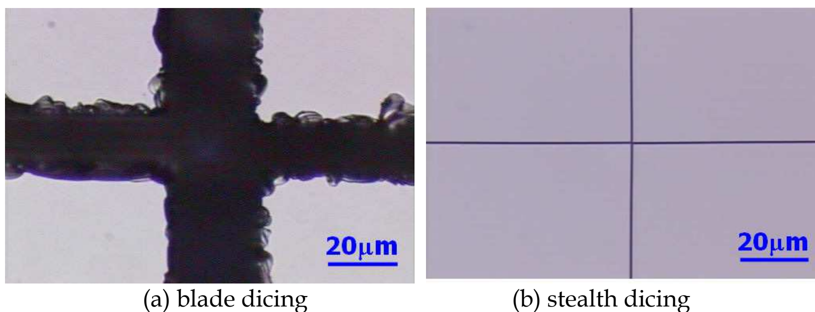

(a) blade dicing (b) stealth dicing

Fig. 4. Comparison of edge quality between blade dicing and SD (Photo: Hamamatsu Photonics K.K.)

In this chapter, heat conduction analysis by considering the temperature dependence of the absorption coefficient is performed for the SD method, and the validity of the analytical result is confirmed by experiment.

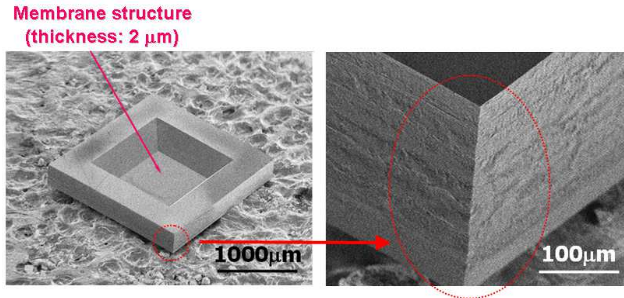

Fig. 5. SD application to actual MEMS device (Photo: Hamamatsu Photonics K.K.)

2. Analysis method

A 1,064 nm laser is considered here, and the internal temperature rise of Si by single pulse irradiation is analyzed (Ohmura et al., 2006). Considering that a laser beam is axisymmetric, we introduce the cylindrical coordinate system $\mathrm{O}-rz$ whose z-axis corresponds to the optical axis of laser beam and r-axis is taken on the surface of Si. The heat conduction equation which should be solved is

$$\rho C_{\mathrm{p}} \frac{\partial T}{\partial t} = \frac{1}{r}\frac{\partial}{\partial r}\left(rK \frac{\partial T}{\partial r} \right) + \frac{\partial}{\partial z}\left(K \frac{\partial T}{\partial z} \right) + w \tag{1}$$

where T is temperature, ρ is density, C_{p} is isopiestic specific heat, K is thermal conductivity, and w is internal heat generation per unit time and unit volume. The finite difference method based on the alternating direction implicit (ADI) method was used for numerical calculation of Eq. (1). The temperature dependence of isopiestic specific heat (Japan Society for Mechanical Engineers ed., 1986) and thermal conductivity (Touloukian et al. ed., 1970) is considered.

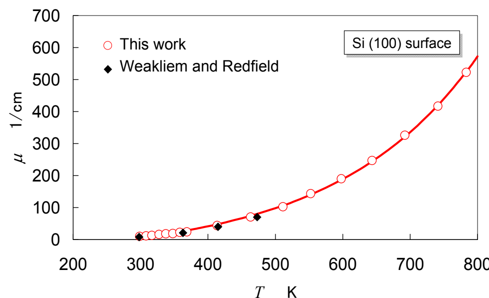

Fig. 6. Temperature dependence of absorption coefficient of silicon single crystal for 1,064 nm

Figure 6 (Fukuyo et al., 2007; Weakliem & Redfield, 1979) shows temperature dependence of the absorption coefficient of single crystal silicon for a wavelength 1,064 nm. The

absorption coefficient $\mu\left(T_{i,j}\right)$ in a lattice (i, j) whose temperature is $T_{i,j}$ is expressed by $\mu_{i,j}$.

When the Lambert law is applied between a small depth Δz from depth $z = z_{j-1}$ to $z = z_j$, the laser intensity $I'_{i,j}$ at the depth $z = z_j$ is expressed by

$$I'_{i,j} = I_{i,j} e^{-\mu_{i,j}\Delta z} \ , \ i = 1, 2, \cdots, i_{\max}, \ j = 1, 2, \cdots, j_{\max} \tag{2}$$

where $I_{i,j}$ is the laser intensity at the depth $z = z_{j-1}$. The measurement values of Fig. 6 are approximated by

$$\mu = 12.991\exp(0.0048244T) - 52.588\exp(-0.0002262T) \quad \left[\mathrm{cm}^{-1}\right] \tag{3}$$

The absorption coefficient of molten silicon is 7.61×10^5 cm^{-1} (Jellison, 1987). Therefore, this value is used for the upper limit of applying Eq. (3).

The $1/e^2$ radius at the depth z of a laser beam which is focused with a lens is expressed by $r_e(z)$. In propagation of light waves from the depth $z = z_{j-1}$ to $z = z_j$, focusing or divergence of a beam can be evaluated by a parameter

$$\gamma_j = \frac{r_e\left(z_j\right)}{r_e\left(z_{j-1}\right)}, \ j = 1, 2, \cdots, j_{\max} \tag{4}$$

The beam is focused when γ_j is less than 1, and is diverged when γ_j is larger than 1. Now, the laser intensity $I_{i,j}$ at the depth $z = z_{j-1}$ of a finite difference grid (i, j) can be expressed by the energy conservation as follows:

1. For $\gamma_{j-1} < 1$

$$I_{i,j} = \frac{\left(\gamma_{j-1}^2 r_i^2 - r_{i-1}^2\right) I'_{i,\,j-1} + \left(1 - \gamma_{j-1}^2\right) r_i^2 I'_{i+1,j-1}}{\gamma_{j-1}^2\left(r_i^2 - r_{i-1}^2\right)}, \ i = 1, 2, \cdots, i_{\max} \tag{5}$$

$$I_{0,j} = I'_{0,\,j-1} + \left(\frac{1}{\gamma_{j-1}^2} - 1\right) I'_{1,\,j-1} \tag{6}$$

2. For $\gamma_{j-1} > 1$

$$I_{i,j} = \frac{\left(\gamma_{j-1}^2 - 1\right) r_{i-1}^2 I'_{i-1,j-1} + \left(r_i^2 - \gamma_{j-1}^2 r_{i-1}^2\right) I'_{i,\,j-1}}{\gamma_{j-1}^2\left(r_i^2 - r_{i-1}^2\right)}, \ i = 1, 2, \cdots, i_{\max} \tag{7}$$

$$I_{0,j} = \frac{I'_{0,\,j-1}}{\gamma_{j-1}^2} \tag{8}$$

Considering Eq. (2), the internal heat generation per unit time and unit volume in the grid (i, j) is given by

$$w_{i,j} = \frac{\left(1 - e^{-\mu_{i,j}\Delta z}\right) I_{i,j}}{\Delta z} \tag{9}$$

In addition, the calculation of the total power at the depth $z = z_{j-1}$ by Eqs. (5) to (8) yields

$$\pi r_0^2 I_{0,j+1} + \sum_{i=1}^{\infty} \pi\left(r_i^2 - r_{i-1}^2\right) I_{i,j+1} = \pi r_0^2 I'_{0,j} + \sum_{i=1}^{\infty} \pi\left(r_i^2 - r_{i-1}^2\right) I'_{i,j} \tag{10}$$

and it can be confirmed that energy is conserved in the both cases of $\gamma_{j-1} < 1$ and $\gamma_{j-1} > 1$.

3. Analysis results and discussions

3.1 The formation mechanism of the inside modified layer

Concrete analyses are conducted under the irradiation conditions that the pulse energy, E_{p0}, is 6.5 μJ, the pulse width (FWHM), τ_{p}, is 150 ns and the minimum spot radius, r_0, is 485 nm. The pulse shape is Gaussian. The pulse center is assumed to occur at $t = 0$. The intensity distribution (spatial distribution) of the beam is assumed to be Gaussian. It is supposed that the thickness of single crystal silicon is 100 μm and the depth of focal plane z_0 is 60 μm. The initial temperature is 293 K.

The analysis region of silicon is a disk such that the radius is 100 μm and the thickness is 100 μm. In the numerical calculation, the inside radius of 20 μm is divided into 400 units at a width 50 nm evenly, and its outside region is divided into 342 units using a logarithmic grid. The thickness is divided into 10,000 units at 10 nm increments evenly in the depth direction. The time step is 20 ps. The boundary condition is assumed to be a thermal radiation boundary.

For comparison with the following analysis results, the temperature dependence of the absorption coefficient is ignored at first, and a value of $\mu = 8.1$ cm^{-1} at room temperature is used. In this case, the time variation of the intensity distribution inside the silicon is given by

$$I(r, z, t) = \sqrt{\frac{\ln 2}{\pi}} \frac{4E_{\mathrm{p}}}{\pi r_e^2(z)\tau_{\mathrm{p}}} \exp\left[-4\ln 2\frac{t^2}{t_{\mathrm{p}}^2} - \frac{2r^2}{r_e^2(z)} - \mu z\right] \tag{11}$$

where E_{p} is an effective pulse energy penetrating silicon and $r_e(z)$ is the spot radius of the Gaussian beam at depth z.

The time variation of temperature at various depths along the central axis is shown in Fig. 7. The maximum temperature distribution is shown in Fig. 8. It is understood from Fig. 7 that the temperature becomes the maximum at time 20 ns at depth of 60 μm which corresponds to the focal position. In Fig. 8, due to reflecting laser absorption, the temperature of the side that is shallower than the focal point of the laser beam is slightly higher. However, the maximum temperature distribution becomes approximately symmetric with respect to the

focal plane. At any rate the maximum temperature rise is about 360 K, which is much smaller than the melting point of 1,690 K under atmospheric pressure (Parker, 2004). It is concluded that polycrystallization after melting and solidification does not occur at all, if the absorption coefficient is independent of the temperature and is the value at the room temperature.

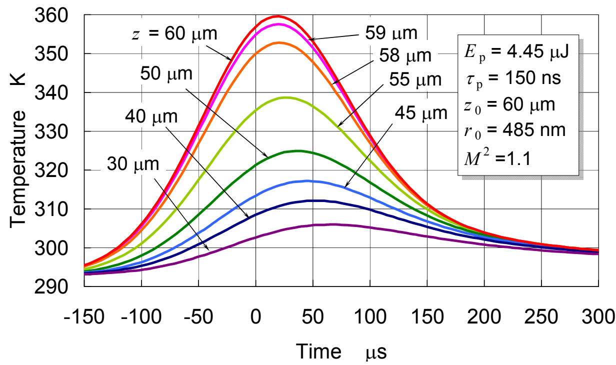

Fig. 7. Time variation of temperature at various depths along the central axis when temperature dependence of absorption coefficient is ignored

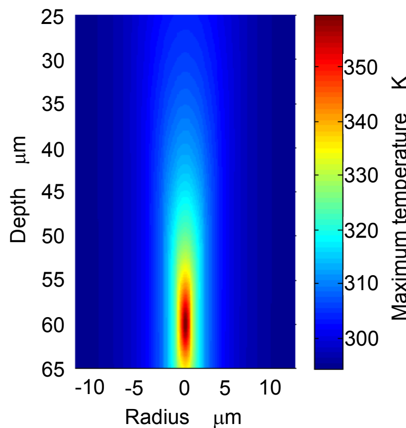

Fig. 8. Maximum temperature distribution when temperature dependence of absorption coefficient is ignored

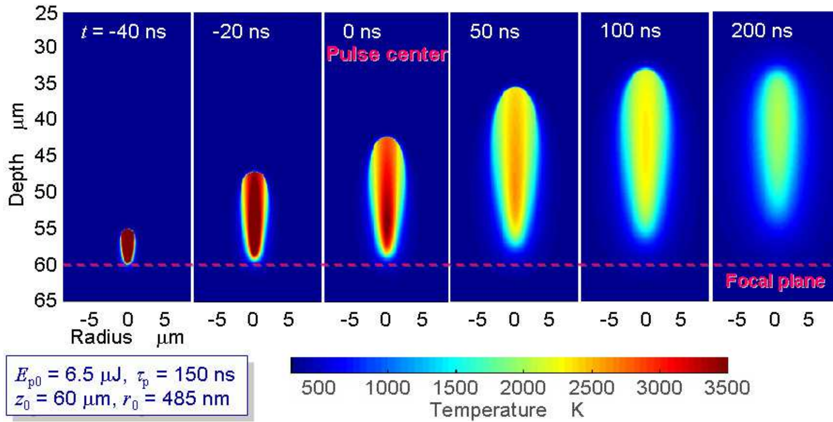

Fig. 9. Time variation of temperature distribution obtained by heat conduction analysis considering the temperature dependence of the absorption coefficient

When the temperature dependence of absorption coefficient (Eq. (3)) is taken into account, the time variation of temperature distribution is shown in Fig. 9. Figure 10 shows the time variation of the temperature distribution along the central axis in Fig. 9. It can be understood from these figures that laser absorption begins suddenly at a depth of $z = 59\ \mu m$ at about $t = -45$ ns and the temperature rises to about 20,000 K instantaneously. The region where the temperature rises beyond 10,000 K will be instantaneously vaporized and a void is formed. High temperature region of about 2,000 K propagates in the direction of the laser irradiation from the vicinity of the focal point as a thermal shock wave. The region where the thermal shock wave propagates becomes a high dislocation density layer due to the shear stress caused by the very large compressive stress.

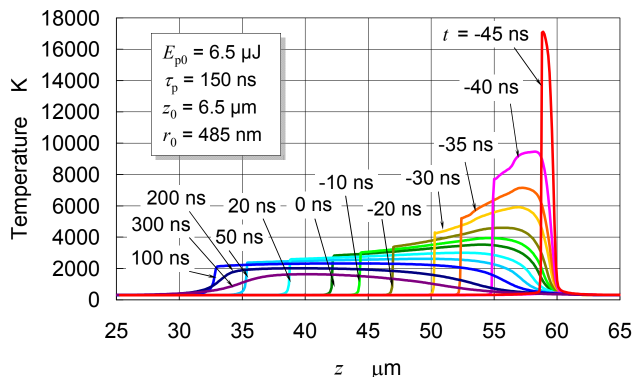

Fig. 10. Time variation of temperature distribution along the central axis

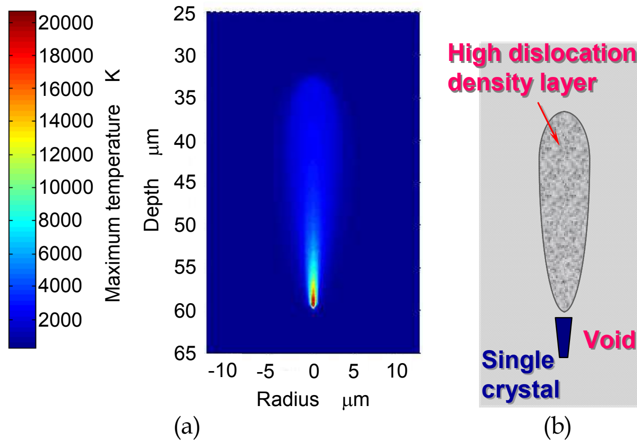

Fig. 11. The maximum temperature distribution (a) and a schematic of SD layer formation (b)

Figure 11 shows the maximum temperature distribution and a schematic of SD layer formation. SD layer looks like an exclamation mark "!". As a result, a train of the high dislocation density layer and void is generated as a belt in the laser scanning direction as shown schematically in Fig. 1. When the thermal shock wave caused by the next laser pulse propagates through part of the high dislocation density layer produced by previous laser pulse, a crack whose initiation is a dislocation progresses. Figure 12 shows a schematic of crack generation by the thermal shock wave. Analyses of internal crack propagation in SD were conducted later using stress intensity factor (Ohmura et al., 2009, 2011).

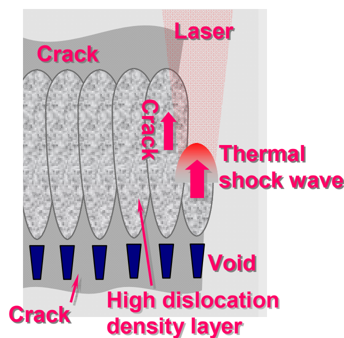

Fig. 12. Schematic of crack generation

Figure 13 shows an inside modified-layer observed by a confocal scanning infrared laser microscope OLYMPUS OLS3000-IR before division (Ohmura et al., 2009). It is confirmed that a train of the high dislocation density layer and void is generated as a belt as estimated in the previous studies. It also can be understood that the internal cracks have been already generated before division.

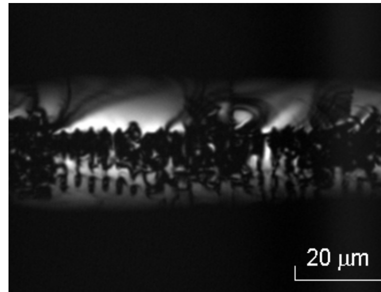

Fig. 13. Confocal scanning IR laser microscopy image before division

3.2 Stealth Dicing of ultra thin silicon wafer

Here heat conduction analysis is performed for the SD method when applied to a silicon wafer of 50 μm thick, and the difference in the processing result depending on the depth of focus is investigated (Ohmura et al., 2007, 2008). Furthermore, the validity of the analytical result is confirmed by experiment. In the analysis, the pulse energy, E_{p0}, is 4 μJ, the pulse width, τ_p, is 150 ns, and the pulse shape is Gaussian. The intensity distribution of the beam is assumed to be Gaussian. It is supposed that the depth of focal plane z_0 is 30 μm, 15 μm and 0 μm. The initial temperature is 293 K.
The analysis region of silicon is a disk such that the radius is 111 μm and the thickness is 50 μm. In the numerical calculation, the inside radius of 11 μm is divided into 440 units at a width 25 nm evenly, and its outside region is divided into 622 units using a logarithmic grid. The thickness is divided into 10,000 units at 5 nm increments evenly in the depth direction. The time step is 10 ps. The boundary condition is assumed to be a thermal radiation boundary.

3.2.1 In the case of focal plane depth 30 μm

The time variation the temperature distribution along the central axis is shown in Fig.14. Figure 14(b) shows the temperature change on a two-dimensional plane of depth and time by contour lines.
It can be understood from Fig. 14(a) that laser absorption begins suddenly at a depth of $z = 29$ μm at about $t = -8$ ns and the temperature rises to about 12,000 K instantaneously. The region where the temperature rises beyond 8,000 K will be instantaneously vaporized and a void is formed. The high temperature area beyond 2,000 K then expands rapidly in the surface direction until $t = 100$ ns as shown in Fig. 14(b). The contour at the leading edge of this high temperature area is clear in this figure. Also the temperature gradient is steep as shown in Fig. 14(a). Therefore, this high-temperature area is named a thermal shock wave as well. It is calculated that the thermal shock wave travels at a mean speed of about 300 m/s.

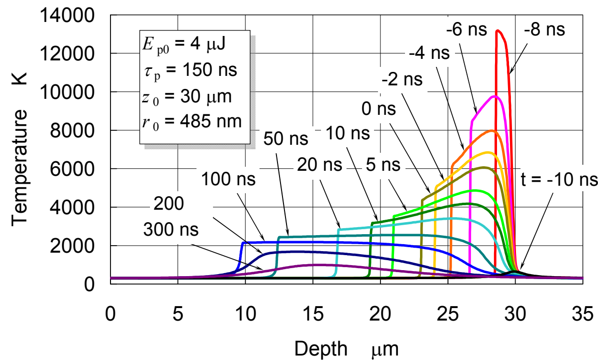

(a)

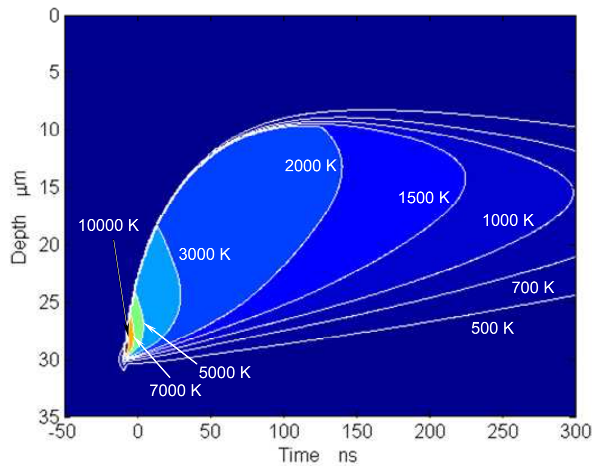

(b)

Fig. 14. Time variation of temperature distribution along the central axis ($z_0 = 30$ μm)

Propagation of the thermal shock wave is shown in Fig. 15 by a time variation of the two-dimensional temperature distribution. The contour of the high-temperature area is comparatively clear until $t = 50$ ns, because the traveling speed of the thermal shock wave is much higher than the velocity of thermal diffusion. The contour of the high temperature area becomes gradually vague at $t = 100$ ns when the thermal shock wave propagation is finished. Because the temperature history is similar to the case of thickness 100 μm, the inside modified layer such as Fig. 3 is expected to be generated.

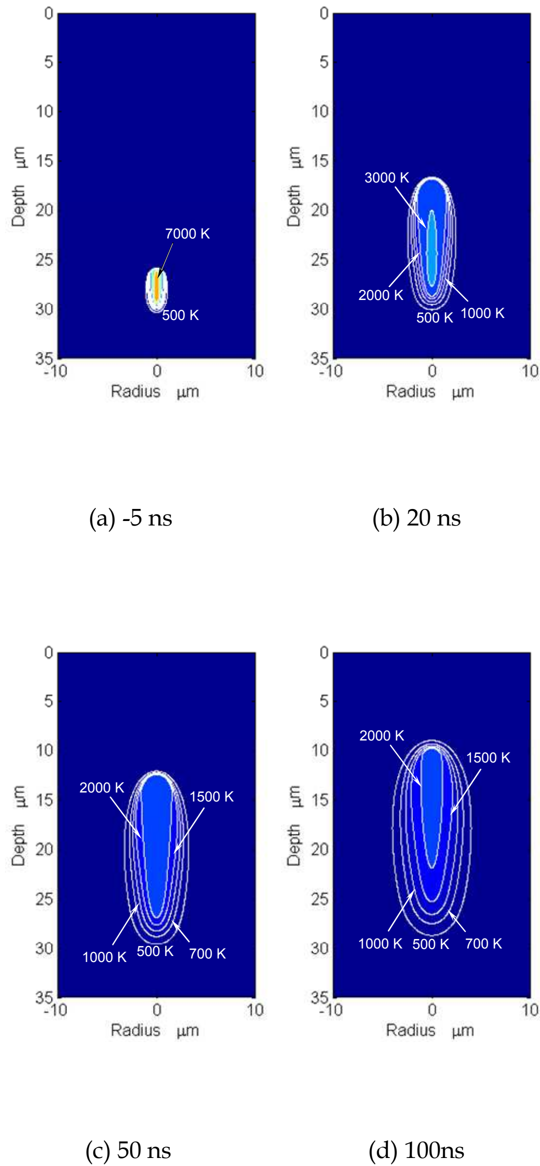

Fig. 15. Time variation of temperature distribution ($z_0 = 30\ \mu m$)

3.2.2 In the case of focal plane depth 15 μm

The time variation of the temperature distribution along the central axis in case of focal plane depth 15 μm is shown in Fig. 16.

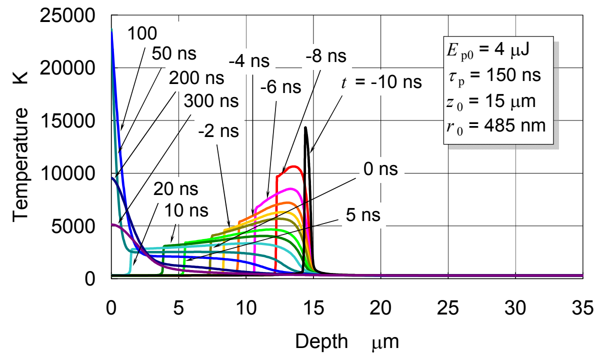

(a)

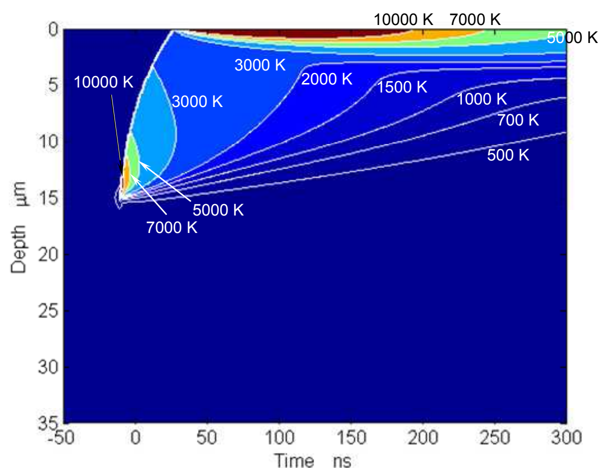

(b)

Fig. 16. Time variation of temperature distribution along the central axis ($z_0 = 15$ μm)

It can be understood from Fig. 16(a) that laser absorption begins suddenly at a depth of $z = 14$ μm at about $t = -10$ ns and the temperature rises to about 12,000 K instantaneously. As well as the case of focal plane depth 30 μm, the region where the temperature rises beyond 8,000 K will be instantaneously vaporized and a void is formed. Then the thermal shock wave propagates in the surface direction until about 25 ns.

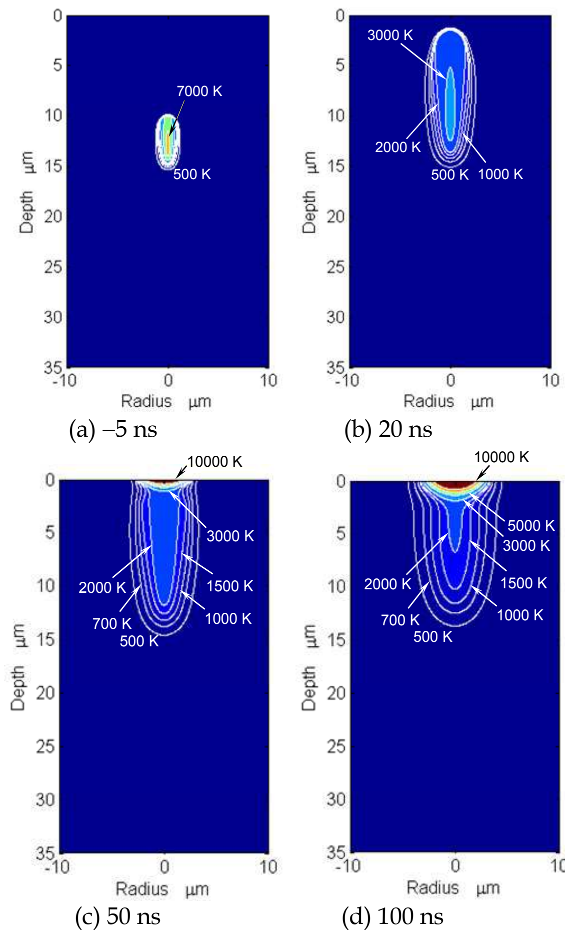

Fig. 17. Time variation of temperature distribution (z_0 = 15 μm)

It is understood from Fig. 16(b) that laser absorption suddenly begins at the surface, once the thermal shock wave reaches the surface. Though the laser power already passes the peak, and gradually decreases, the surface temperature rises beyond 20000 K, which is higher than the maximum temperature which is reached at the inside. Although the thermal diffusion velocity is fairly slower than the thermal shock wave velocity, the internal heat is diffused to the surrounding. However, because the heat in the neighborhood of the surface is diffused only in the inside of the lower half, the surface temperature becomes very high and is maintained comparatively for a long time. Ablation occurs of course in such a high-temperature state. As a result, it is expected that not only is an inside modified layer generated, but also the surface is removed by ablation. Figure 17 shows that the surface temperature rises suddenly after the thermal shock wave propagates in the inside of the silicon, and reaches the surface, by the time variation of two dimensional temperature distribution.

3.2.3 In the case of focal plane depth 0 μm

When the laser is focused at the surface, as shown in Fig. 18, laser absorption begins suddenly at the surface at $t = -35$ ns, and the maximum surface temperature in the calculation reaches 6×10^5 K. It is estimated that violent ablation occurs when such an ultra-high temperature is reached. Because of the pollution of the device area by the scattering of the debris and thermal effect, the ablation at the surface is quite unfavorable.

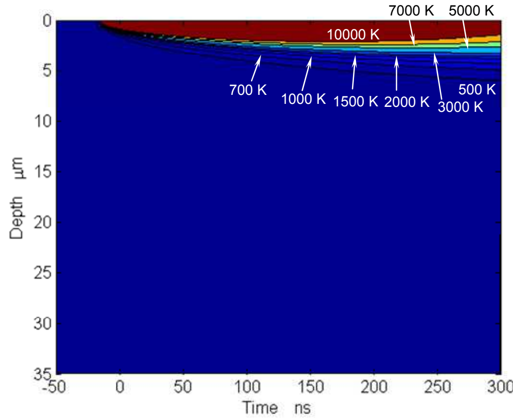

Fig. 18. Time variation of temperature distribution along the central axis ($z_0 = 0$ μm)

3.2.4 Comparison of the maximum temperature distributions and the experimental results

The maximum temperature distributions at the focal plane depths of 30 μm, 15 μm and 0 μm are shown in Fig. 19 in order to compare the previous analysis results at a glance.

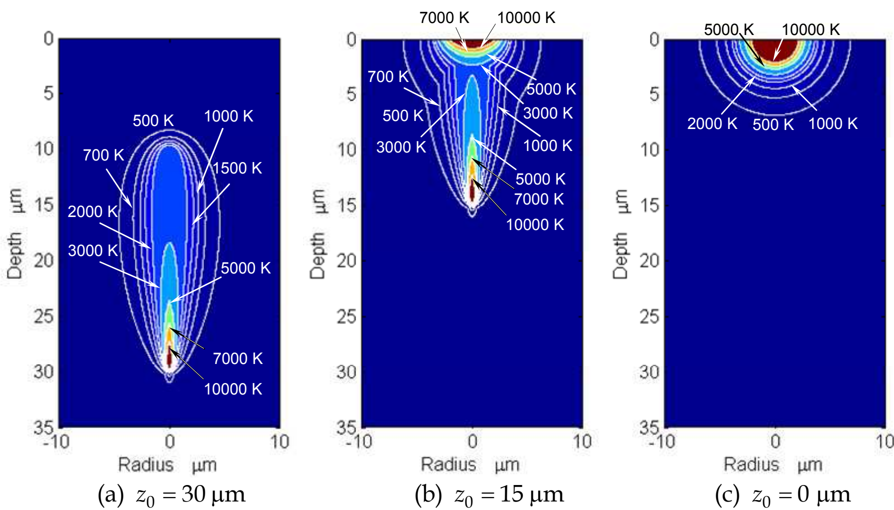

Fig. 19. Comparison of the maximum temperature distribution

Because high-temperature area stays in the inside of the wafer when z_0 is 30 μm, it was estimated that the inside modified layer as shown in Fig. 3 will be generated. In the case of $z_0 = 15$ μm, it was estimated that the surface is ablated although the modified layer is generated inside. In the case of $z_0 = 0$ μm, it was estimated that the surface was ablated intensely. It is concluded from the above analysis results that the laser irradiation condition for SD processing should be selected at a suitable focal plane depth so that the thermal shock wave does not reach the surface.

In order to verify the validity of the estimated results, laser processing experiments were conducted under the same irradiation condition as the analysis condition. The repetition rate in the experiments was 80 kHz. The results are shown in Fig. 20. Optical microscope photographs of the top views of the laser-irradiated surfaces and the divided faces are shown in the middle row and the bottom row, respectively. Figures 20 (a), (b) and (c) are results in the case of $z_0 = 30$ μm, $z_0 = 15$ μm, $z_0 = 0$ μm, respectively.

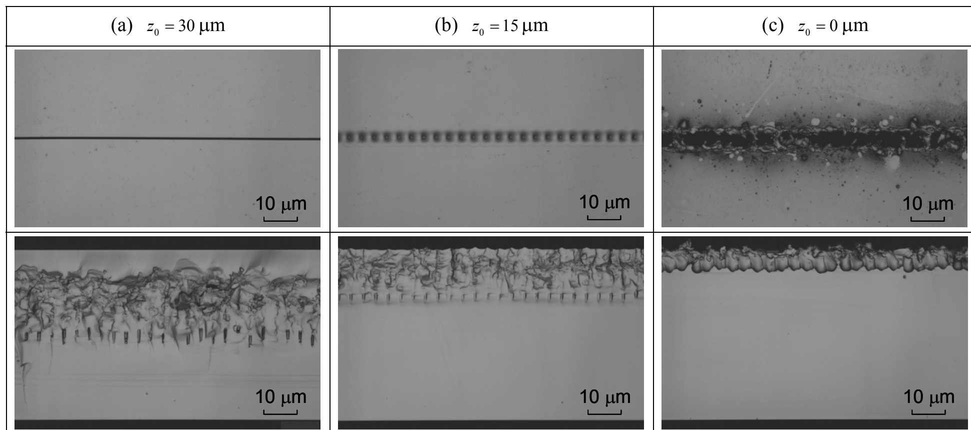

Fig. 20. Experimental results ($E_{p0} = 4$ μJ, $\tau_p = 150$ ns, $v = 300$ μm/s, $f_p = 80$ kHz)

In the case of $z_0 = 30$ μm which is shown in Fig. 20 (a), it can be confirmed that voids are generated at the place that is slightly higher than the focal plane and the high dislocation density layer is generated in those upper parts, which are similar to Fig. 3. In the case of $z_0 = 15$ μm which is shown in Fig. 20 (b), it is recognized that voids are generated at the place that is slightly higher than the focal plane and the high dislocation density layer is generated in those upper parts. However, it is observed that the surface is ablated and holes are opened from the photograph of the laser irradiated surface. In the case of $z_0 = 0$ μm which is shown in Fig. 20 (c), it is seen that strong ablation occurs and debris is scattered to the surroundings. Voids and the high dislocation density layer are not recognized in the divided face. Only the cross section of the hole caused by ablation is seen. These experimental results agree fairly well with the estimation based on the previous analysis

result. Therefore, the validity of the analytical model, the analysis method, and the analysis results of this study are proven. The processing results can be estimated to some extent by using the analysis model and the analysis method in the present study. It is useful in optimization of the laser irradiation condition.

4. Conclusion

In the stealth dicing (SD) method, the laser beam that is permeable for silicon is absorbed locally in the vicinity of the focal point, and an interior modified layer (SD layer), which consists of voids and high dislocation density layer, is formed. In this chapter, it was clarified by our first analysis that the above formation was caused by the temperature dependence of the absorption coefficient and the propagation of a thermal shock wave. Then, the SD processing results of an ultra thin wafer of 50 μm in thickness were estimated based on this analytical model and analysis method. Particularly we paid attention to the difference in the results depending on the focal plane depth. Furthermore, in order to compare with the analysis results, laser processing experiments were conducted with the same irradiation condition as the analysis conditions.

In the case of focal plane depth $z_0 = 30$ μm, the analysis result of temperature history was similar to the case when the wafer thickness is 100 μm and the focal plane depth is 60 μm. Therefore, it was predicted that a similar inside modified layer will be generated. In the case of $z_0 = 15$ μm, it was estimated that not only the inside modified layer is generated, but also the surface is ablated. Because the thermal shock wave reached the surface, remarkable laser absorption occurred at the surface. In the case of $z_0 = 0$ μm, it was estimated that the surface is ablated intensely. These estimation results agreed well with experimental results. Therefore, the validity of the analytical model, the analysis method and the analysis results of this study was proven.

As conclusion of this chapter, the following points became clear:

1. When the analytical model and the analysis method of the present study are used, the processing mechanism can be understood well, and the processing results can be estimated to some extent. It is useful in optimization of the laser irradiation condition.
2. There is a suitable focal plane depth in the SD processing, and it is necessary to select the laser irradiation condition so that the thermal shock wave does not reach the surface.

5. References

Fukumitsu, K., Kumagai, M., Ohmura, E., Morita, H., Atsumi, K., Uchiyama, N. (2006). The Mechanism of Semi-Conductor Wafer Dicing by Stealth Dicing Technology, *Online Proceedins of 4th International Congress on Laser Advanced Materials Processing (LAMP2006)*, Kyoto, Japan, May 16-19, 2006

Fukuyo, F., Fukumitsu, K., Uchiyama, N. (2005). The Stealth Dicing Technologies and Their Application, *Proceedings of 6th Internaitonal Symposium onLaser Precision Micro-Fabrication (LPM2005)*, Williamsburg, USA, April 4-7, 2005

Fukuyo, F., Ohmura, E., Fukumitsu, K., Morita, H. (2007). Measurement of Temperature Dependence of Absorption Coefficient of Single Crystal Silicon, *Journal of Japan Laser Processing Society*, Vol.14, No.1 (January 2007), pp. 24-29, ISSN 1881-6797 (in Japanese)

Japan Society for Mechanical Engineers (Eds.) (1986). *JSME Data Book: Heat Transfer, 4th ed.*, Japan Society for Mechanical Engineers, ISBN 978-4-88898-041-8, Tokyo, Japan (in Japanese)

Jellison, Jr. G.E. (1987). Measurements of the Optical Properties of Liquid Silicon and Germanium Using Nanosecond Time-Eesolved Ellipsometry, *Applied Physics Letters*, Vol.51, No.5 (August 1987), pp. 352-354, ISSN 0003-6951

Kumagai, M., Uchiyama, N., Ohmura, E., Sugiura, R., Atsumi, K., Fukumitsu, K. (2007). Advanced Dicing Technology for Semiconductor Wafer —Stealth Dicing—, *IEEE Transactions on Semiconductor Manufacturing*, Vol.20, No.3 (August 2007) pp. 259-265, ISSN 0894-6507

Ohmura, E., Fukumitsu, K., Uchiyama, N., Atsumi, K., Kumagai, M., Morita, H. (2006). Analysis of Modified Layer Formation into Silicon Wafer by Permeable Nanosecond Laser, *Proceedings of the 25th International Congress on Application of Laser and Electro-Optics (ICALEO2006)*, pp. 24-31, ISBN #0-912035-85-4, Scottsdale, USA, October 30-November 2, 2006

Ohmura, E., Fukuyo, F., Fukumitsu, K., Morita, H. (2006). Internal Modified-Layer Formation Mechanism into Silicon with Nanosecond Laser, *Journal of Achievements in Materials and Manufacturing Engineering*, Vol.17, No.1/2 (July 2006), pp. 381-384, ISSN 1734-8412

Ohmura, E., Kawahito, Y., Fukumitsu, K., Okuma, J., Morita, H. (2011). Analysis of Internal Crack Propagation in Silicon Due to Permeable Laser Irradiation —Study on Processing Mechanism of Stealth Dicing, *Journal of Materials Science and Engineering, A*, Vol.1, No.1, (June 2011), pp. 46-52, ISSN 2161-6213

Ohmura, E., Kumagai, M., Nakano, M., Kuno, K., Fukumitsu, K., Morita, H. (2007). Analysis of Processing Mechanism in Stealth Dicing of Ultra Thin Silicon Wafer, *Proceedings of the International Conference on Leading Edge Manufacturing in 21st Century (LEM21)*, pp. 861-866, Fukuoka Japan, November 7-9, 2007

Ohmura, E., Kumagai, M., Nakano, M., Kuno, K., Fukumitsu, K., Morita, H. (2008). Analysis of Processing Mechanism in Stealth Dicing of Ultra Thin Silicon Wafer, *Journal of Advanced Mechanical Design, Systems, and Manufacturing*, Vol.2, No.4 (March 2008) pp. 540-549, ISSN 1881-3054

Ohmura, E., Ogawa, K., Kumagai, M., Nakano, M., Fukumitsu, K., Morita, H. (2009). Analysis of Crack Propagation in Stealth Dicing Using Stress Intensity Factor, *On-line Proceedings of the 5th International Congress on Laser Advanced Materials Processing (LAMP2009)*, Kobe, Japan, June 29-July 2, 2009

Parker, S.P. et al. (Eds.) (2004). *Dictionary of Physics, 2nd ed.*, McGraw-Hill, ISBN 0-07-052429-7, New York, USA

Touloukian, Y.S., Powell, R.W., Ho, C.Y., Klemens, P.G. (Eds.) (1970). *Thermal Conductivity: Metallic Elements and Alloys*, IFI/Plenum, ISBN 306-67021-6, New York, USA

Weakliem, H.A. & Redfield, D. (1979). Temperature Dependence of the Optical Properties of Silicon, *Journal of Applied Physics*, Vol.50, No.3 (March 1979), pp. 1491-1493, ISSN 0021-8979

Heat Transfer - Engineering Applications
Edited by Prof. Vyacheslav Vikhrenko

ISBN 978-953-307-361-3
Hard cover, 400 pages
Publisher InTech
Published online 22, December, 2011
Published in print edition December, 2011

Heat transfer is involved in numerous industrial technologies. This interdisciplinary book comprises 16 chapters dealing with combined action of heat transfer and concomitant processes. Five chapters of its first section discuss heat effects due to laser, ion and plasma-solid interaction. In eight chapters of the second section engineering applications of heat conduction equations to the curing reaction kinetics in manufacturing process, their combination with mass transport or ohmic and dielectric losses, heat conduction in metallic porous media and power cables are considered. Analysis of the safety of mine hoist under influence of heat produced by mechanical friction, heat transfer in boilers and internal combustion engine chambers, management for ultrahigh strength steel manufacturing are described in this section as well. Three chapters of the last third section are devoted to air cooling of electronic devices.

How to reference
In order to correctly reference this scholarly work, feel free to copy and paste the following:

Etsuji Ohmura (2011). Temperature Rise of Silicon Due to Absorption of Permeable Pulse Laser, Heat Transfer - Engineering Applications, Prof. Vyacheslav Vikhrenko (Ed.), ISBN: 978-953-307-361-3, InTech, Available from: http://www.intechopen.com/books/heat-transfer-engineering-applications/temperature-rise-of-silicon-due-to-absorption-of-permeable-pulse-laser

INTECH
open science | open minds

InTech Europe
University Campus STeP Ri
Slavka Krautzeka 83/A
51000 Rijeka, Croatia
Phone: +385 (51) 770 447
Fax: +385 (51) 686 166
www.intechopen.com

InTech China
Unit 405, Office Block, Hotel Equatorial Shanghai
No.65, Yan An Road (West), Shanghai, 200040, China
中国上海市延安西路65号上海国际贵都大饭店办公楼405单元
Phone: +86-21-62489820
Fax: +86-21-62489821

© 2011 The Author(s). Licensee IntechOpen. This is an open access article distributed under the terms of the Creative Commons Attribution 3.0 License, which permits unrestricted use, distribution, and reproduction in any medium, provided the original work is properly cited.